

## Positron studies of defects in ion-implanted SiC

G. Brauer and W. Anwand

*Arbeitsgruppe Positronen-Annihilations-Spektroskopie der Technische Universität Dresden,  
c/o Forschungszentrum Rossendorf, Postfach 510119, D-01314 Dresden, Germany*

P. G. Coleman and A. P. Knights

*School of Physics, University of East Anglia, Norwich NR4 7TJ, United Kingdom*

F. Plazaola

*Elektrika eta Elektronika Saila, Euskal Herriko Unibertsitatea, 644 p.k., 48080 Bilbo, Spain*

Y. Pacaud and W. Skorupa

*Institut für Ionenstrahlphysik und Materialforschung, Forschungszentrum Rossendorf, Postfach 510119, D-01314 Dresden, Germany*

J. Störmer and P. Willutzki

*Institut für Nukleare Festkörperphysik, Universität der Bundeswehr München, D-85577 Neubiberg, Germany*

(Received 4 January 1996; revised manuscript received 15 April 1996)

Radiation damage caused by the implantation of 200 keV Ge<sup>+</sup> ions into 6H-SiC has been studied by monoenergetic positron Doppler broadening and lifetime techniques. Specimens exposed to seven ion fluences ranging from 10<sup>16</sup> to 10<sup>19</sup> m<sup>-2</sup>, together with unirradiated samples, were studied. The depth of the damaged crystalline layer was found to range from about 300 to 600 nm and, for ion fluences above 3 × 10<sup>17</sup> m<sup>-2</sup>, an amorphous layer is seen whose thickness increases to 133 nm at the highest fluence. Positron lifetime measurements, in combination with theoretical calculations, suggest that the main defect produced is the divacancy, but that Si monovacancies are also created. In the amorphous surface layer larger agglomerates consisting of at least four but more probably six vacancies are detected. Trapping rates are evaluated as a function of incident positron energy by applying the positron trapping model to the data. Values for defect concentrations in the damaged layers of about 50 ppm are deduced by invoking plausible assumptions; the problem of extracting defect profiles from the data is discussed. [S0163-1829(96)00230-5]

### I. INTRODUCTION

The current interest in silicon carbide (SiC) as a semiconductor for high-temperature, high-power, high-frequency, and radiation-resistant device technology is based on its outstanding chemical, mechanical, thermal, and electronic properties. Nowadays it is already possible to grow SiC with good enough perfection and control to develop excellent devices. In order to improve the device performance and wafer die yields, it is necessary to characterize thoroughly the starting material with respect to its electrical and optical properties as well as to establish a microscopic understanding of defects. The identification of the chemical nature or atomic and electronic structure of defects in SiC is in its early stages.<sup>1,2</sup>

SiC appears in many different crystallographic structures (polytypes) providing a lone cubic (3C), a great number of hexagonal (2H, 4H, 6H, . . .) as well as rhombohedral structures (15R, 21R, . . .). The 3C, 4H, and 6H polytypes of SiC are the most important for device applications. Although the arrangement of next neighbors is the same for each Si and C atom in all polytypes, the second- and third-neighbor shell may result in slightly altered arrangements leading to crystallographically inequivalent lattice sites [e.g., in 3C, one cubic (k); in 4H, one cubic (k) and one hexagonal (h); in 6H, two cubic (k<sub>1</sub>, k<sub>2</sub>) and one hexagonal (h)].<sup>1</sup> It is generally

expected that impurities residing at inequivalent lattice sites of a particular polytype may reveal different electronic properties due to the Kohn-Luttinger effect.<sup>3</sup>

Positron annihilation spectroscopy (PAS) is now a well-established tool for the study of electronic and defect properties of solids.<sup>4,5</sup> Recent developments in slow positron beam methods<sup>6</sup> allow the investigation of such properties for thin films, layered structures, and at surfaces.<sup>7</sup> PAS is mostly applied to, and best understood in, metallic materials, but has also found its role in the study of defects in semiconductors; it has, for example, revealed information on ion-type acceptors via positron trapping at shallow Rydberg states.<sup>8</sup> To date mainly elemental and compound (III-V, II-VI) semiconductors have been investigated, but recently there has been an increased interest in SiC.<sup>9-16</sup>

Pure SiC is a highly stoichiometric compound without intrinsic vacancies. Up to temperatures of 2000 K no indication of thermal vacancy formation can be detected by PAS.<sup>9</sup> From positron lifetime measurements on single-crystal SiC wafers a bulk lifetime  $\tau_b = (150 \pm 2)$  ps has been measured for both 4H and 6H polytypes<sup>10</sup> and  $(144 \pm 1)$  ps for *n*- or *p*-type 6H-SiC.<sup>11</sup> All specimens studied in Refs. 10 and 11 exhibited a second, obviously defect-related lifetime component with rather low intensity ranging from 250 ps to about 350 ps. Not unexpectedly, a more complex defect structure is indicated in sintered nanocrystalline SiC.<sup>10</sup> It is clear that at

present no conclusive interpretation of the defect characteristics of as-grown bulk or nanocrystalline SiC can be given.

Slow positron beam experiments have been performed in order to study chemical vapor deposited SiC thin films on Si substrate through variations in the Doppler broadening parameter  $S$ . It was found that the positrons are very sensitive to changes in important film parameters as a function of the deposition conditions.<sup>10</sup> Other authors reported the results of 1-MeV electron bombardment of  $n$ -type 3C-SiC thin films grown epitaxially on Si (100).<sup>12</sup> They found that above a critical fluence of about  $5 \times 10^{20} \text{ m}^{-2}$  monovacancies at Si sublattice sites ( $V_{\text{Si}}$ ) are created, along with divacancies generated via the combination between  $V_{\text{Si}}$  and  $V_{\text{C}}$  monovacancies on the C sublattice.

Positron lifetime measurements have been used in order to characterize atomic defects in SiC introduced by particle irradiation, and their evolution during subsequent isochronal annealing.<sup>11,13–16</sup> No effect of 2.2-MeV electron irradiation of  $p$ -type 6H-SiC up to a fluence of  $6 \times 10^{21} \text{ m}^{-2}$  could be found,<sup>11,16</sup> probably due to the positive charge of vacancies produced, whereas in  $n$ -type 6H-SiC the same irradiation (and for  $E = 10 \text{ MeV}$  at  $1.2 \times 10^{22} \text{ m}^{-2}$ ) resulted in longer lifetime components of 160 and 260 ps. The shorter lifetime was attributed to the neutral C vacancy  $V_{\text{C}}$  and the longer one to the silicon vacancy  $V_{\text{Si}}$ .

Low-temperature (80 K) electron irradiation of  $n$ -type 6H-SiC single crystals with different energies  $E$  and fluences  $\Phi$  was found to produce different types of defects.<sup>14,15</sup> In the unirradiated material a mean positron lifetime  $\bar{\tau} = (146 \pm 2) \text{ ps}$  was reported, which is regarded to represent the bulk value  $\tau_b$ . A small increase in  $\bar{\tau}$  to  $159 \pm 4 \text{ ps}$  occurred after 0.47 MeV electron irradiation, whereas  $\bar{\tau}$  increased to  $210 \pm 29 \text{ ps}$  after 2.5 MeV irradiation. In the latter case the long lifetime is found if a decomposition of the positron lifetime spectra into two components is performed. The intensity  $I_2$  of the long-lived component increased with increasing fluence, up to 100% at the highest fluence. These findings, coupled with observations of annealing behavior, are interpreted as positron trapping in  $V_{\text{Si}}$  (lower electron energy) and in a complex of the divacancy  $V_2$  coupled to antisite atoms (higher electron energy).

Other authors<sup>13</sup> reported the bombardment of different  $n$ -type polytypes of SiC single crystals with 4-MeV electrons, reactor neutrons and 124-MeV  $^{129}\text{Xe}$  ions. The bulk lifetime  $\tau_b$  found in this study for all the SiC polytypes studied (irrespective of  $N$  concentration) was  $157 \pm 2 \text{ ps}$ ; this value is somewhat higher than that reported above, perhaps because of a somewhat broader time resolution. This introduction of defects into the SiC by irradiation always increases the observed single (mean) lifetime, reaching saturation level as the fluence is increased. The cascade model of defect formation has been applied to describe and to interpret this behavior. Vacancy cluster formation is observed during annealing at temperatures up to  $2300 \text{ }^\circ\text{C}$ ; their size, concentration and thermal stability is found to depend on both the type of irradiation and the applied fluence.

SiC is a difficult material to synthesize and many techniques have been used. It is also very difficult to process because of the high stability of lattice defects and its high temperature of recrystallization [about  $1450 \text{ }^\circ\text{C}$  (Ref. 17)]. Recently it has been shown that it is possible to lower this

temperature down to  $480 \text{ }^\circ\text{C}$  with the help of ion beam induced epitaxial crystallization (IBIEC).<sup>18</sup> Unfortunately, the recrystallization was found to be incomplete because the re-growth process is stopped by polynucleation in the near surface region. The role of Ge, together with the defects induced by Ge ion irradiation, seems to be important to the understanding of the IBIEC phenomena.

The aim of the present work is to study the radiation damage in 6H-SiC due to the implantation of 200-keV  $\text{Ge}^+$  ions in the fluence range  $10^{16} - 10^{19} \text{ m}^{-2}$  and to characterize this damage both experimentally (by PAS) and theoretically. In Sec. II experimental details of the work are described, and in Sec. III theoretical calculations of the positron lifetime in some SiC polytypes, and a discussion of the variable-energy positron measurements, are presented. Conclusions are presented in Sec. IV.

## II. EXPERIMENTAL METHODS

Two 25-mm-diam single-crystal  $n$ -type 6H-SiC wafers with (0001) orientation (Si surface) (Ref. 17) were used as substrate materials. Both wafers were cut into four equally sized pieces; seven pieces (labeled EU1 – EU7) were implanted with 200-keV  $\text{Ge}^+$  ions at room temperature with fluences  $\Phi$  ranging from  $10^{16}$  to  $10^{19} \text{ m}^{-2}$  and one piece (EU0) was kept as a virgin reference specimen. The ion fluences for specimens EU1–7 were 1, 3, 10, 30, 100, 300, and  $1000 \times 10^{16} \text{ m}^{-2}$ , respectively. After implantation the color of the specimens changed from light green (virgin material) to light khaki brown (highest fluence).

Room-temperature variable-energy positron measurements were performed for all specimens using a computer-controlled magnetic-transport beam system at UEA Norwich.<sup>20</sup> Photopeak energy spectra of annihilation  $\gamma$  rays were measured as a function of incident positron energy  $E$  with a Ge detector having an energy resolution (FWHM) of about 1.2 keV at 511 keV. The Doppler broadening of the annihilation radiation is caused by the momentum of the annihilating electron-positron pair and can be characterized by the line-shape parameter  $S$ .  $S$  is defined (after background corrections) as the integral of  $\gamma$ -ray intensity in the central energy region divided by the total intensity of the line.  $S(E)$  is commonly fitted by a program such as VEPFIT (Ref. 21) to yield defect profiles, damaged layer thicknesses, etc.

Variable-energy positron lifetime measurements were performed on selected specimens [EU3, EU7, virgin 6H-SiC (not identical with EU0)] with the timed beam system at UBW München<sup>22</sup> at room temperature.  $\tau(E)$  yields the same information as  $S(E)$ , but provides useful additional information about the type of defects involved.

## III. RESULTS AND DISCUSSION

### A. Theoretical calculations of positron lifetimes

In order to have an idea of the positron lifetimes to be expected in SiC polytypes calculations using the superimposed atom model<sup>23</sup> have been performed for perfect and several defected lattices. In the calculations the positron does not affect the electronic structure beyond the short-range enhancement of the electron density at the positron. For delocalized positron states this is the correct limit of the two-

component density-functional theory<sup>24</sup> used to describe electron-positron systems. In the case of a localized positron state at a defect the positron density affects also the average electron density, and the electron and positron densities should be calculated simultaneously and self-consistently within the two-component density-functional theory. However, the approximation made in the calculation of the positron annihilation lifetimes is not very severe, because neglecting the accumulation of the average electron density is compensated by a stronger short-range enhancement of the electron density.<sup>24</sup>

A more severe approximation, which has been made here, is that the relaxation of the atoms surrounding the vacancy defects is not taken into account. The superimposed atom model retains the three-dimensional character of the atomic arrangement and the positron state. The electron density  $n_-(\mathbf{r})$  and the Coulomb potential  $V_C(\mathbf{r})$  of the host system are obtained from the free-atom densities and potentials as

$$n_-(\mathbf{r}) = \sum_i n^{\text{at}}(|\mathbf{r} - \mathbf{R}_i|)$$

and

$$V_C(\mathbf{r}) = \sum_i V_C^{\text{at}}(|\mathbf{r} - \mathbf{R}_i|). \quad (1)$$

The summations run over the occupied atomic sites, and  $n^{\text{at}}$  and  $V_C^{\text{at}}$  are the atomic electron density and Coulomb potential, respectively. Thus, the electron density and the Coulomb potential for the solid are non-self-consistent. The three-dimensional potential  $V_+(\mathbf{r})$  felt by the positron is then constructed as a sum of the electrostatic potential  $V_C(\mathbf{r})$  due to the nuclei and the electrons, and a correlation potential  $V_{\text{corr}}$  describing electron-positron correlation effects, i.e.,

$$V_+(\mathbf{r}) = V_C(\mathbf{r}) + V_{\text{corr}}[n_-(\mathbf{r})]. \quad (2)$$

Within the local-density approximation (LDA),  $V_{\text{corr}}$  depends on the local electron density unperturbed by the positron. For the density dependence of  $V_{\text{corr}}$  a parametrization<sup>24</sup> based on many-body results<sup>25</sup> has been used. The free-atom electron densities needed for the construction have been calculated by a self-consistent density-functional program employing LDA for the electron exchange and correlation.<sup>26,27</sup>

The calculations of positron states by the atomic superposition method have been performed by the supercell approach, employing periodic boundary conditions for the positron wave function. The supercells used in the calculations depend on the SiC polytype.

In the case of 3C-SiC (zinc-blende structure) the supercell is a cube containing 8 atoms in the perfect lattice. In the case of a monovacancy and a divacancy it contains 63 and 62 atoms, respectively. For vacancy clusters of 4, 6, and 8 vacancies supercells containing 212, 210, and 208 atoms, respectively, have been used, in order to avoid the possible interaction between defects that may occur due to the periodicity of the boundary conditions used in the supercell calculations. However, it has been found that using supercells containing only 60, 58, and 56 atoms for the same vacancy clusters, the obtained lifetimes are within 3 ps of those obtained with the larger supercells. In the case of 2H-SiC an

TABLE I. Data for the SiC polytypes used in the calculations. The lattice constants  $a$  and  $c$  (given in atomic units, 1 a.u. =  $0.529\,177 \times 10^{-10}$  m) have been taken from Ref. 27. The values  $\tau_{\text{LDA}}$  correspond to the theoretical bulk lifetimes calculated within the LDA.

Host	$a$ [a.u.]	$c$ [a.u.]	$\tau_{\text{LDA}}$ [ps]
3C-SiC	8.24	-	141
2H-SiC	5.81	9.54	142
6H-SiC	5.81	28.50	141

orthorhombic supercell containing 8 atoms has been used in order to simulate its hexagonal structure.<sup>28</sup> For mono- and divacancies the supercell contains 63 and 62 atoms, respectively.

To simulate the more complicated structure of 6H-SiC,<sup>28</sup> the orthorhombic supercell used for the perfect lattice calculations contains 24 atoms, and the supercell used to calculate the lifetime in mono- and divacancies contains 95 and 94 atoms, respectively.

The positron potential [Eq. (2)] is calculated at the nodes of a three-dimensional mesh within the supercell. The Schrödinger equation is discretized, and the positron wave function at the mesh points of the supercell and the positron energy eigenvalue are solved iteratively by a numerical relaxation method.<sup>29</sup> It was found that the results were essentially insensitive to the density of mesh points; for example, the variation in positron lifetime calculated using mesh point densities ranging from 7 to  $21 \times 10^{-12}$  a.u.<sup>-3</sup> is only 0.5 ps.

The positron annihilation rate  $\lambda$  is calculated using the LDA as

$$\lambda_{\text{LDA}} = 1/\tau_{\text{LDA}} = \int d\mathbf{r} |\Psi_+(\mathbf{r})|^2 \Gamma[n_-(\mathbf{r})]. \quad (3)$$

Here  $|\Psi_+(\mathbf{r})|^2$  is the positron density and  $\Gamma(n)$  denotes the annihilation rate for a positron in a homogeneous electron gas. In the calculations for  $\Gamma(n)$  an interpolation formula,<sup>24</sup> modified in order to take into account the lack of complete positron screening in semiconductors,<sup>30</sup> is used:

$$\Gamma[n(\mathbf{r})] = \pi r_0^2 c n [1 + 1.23 r_s + 0.8295 r_s^{3/2} - 1.26 r_s^2 + 0.3286 r_s^{5/2} + (1 - 1/\epsilon_\infty) r_s^3 / 6]. \quad (4)$$

Here  $r_0$  is the classical electron radius,  $c$  the velocity of light,  $r_s = (3/4\pi n)^{1/3}$ , and  $\epsilon_\infty$  is the high-frequency dielectric constant which takes the values 6.52 and 6.70 for 3C-SiC and 6H-SiC, respectively.<sup>31</sup>

All results of the calculations are summarized in Tables I and II. The lifetimes in both tables are based on  $\epsilon_\infty = 6.70$ . If  $\epsilon_\infty = 6.52$  is used no appreciable change in the lifetimes obtained ( $\leq 1$  ps) is noticed. Even though the structures of the three polytypes used in the calculations are different, the calculated bulk lifetimes (see Table I) are the same to within 1 ps. However, this result is not unexpected because the volume per atom in the three structures is very similar. Moreover, the calculated bulk lifetime is in fairly good agreement with the experimental lifetime values obtained in this work (see Sec. III C) and by other researchers.<sup>11,14-16</sup>

TABLE II. Calculated positron lifetimes  $\tau_d$  in different types of neutral and unrelaxed vacancy-type defects in three SiC polytypes. The defect configuration  $n$ - $V_{\text{Si}}V_{\text{C}}$  ( $n=1,2,3,4$ ) indicates a vacancy agglomerate with  $n$  divacancies.  $E_b$  indicates the binding energy of the positron in the corresponding defect.

Defect	3C-SiC		2H-SiC		6H-SiC	
	$\tau_d$ [ps]	$E_b$ [eV]	$\tau_d$ [ps]	$E_b$ [eV]	$\tau_d$ (ps)	$E_b$ (eV)
$V_{\text{C}}$	150	0.28	151	0.26	150	0.28
$V_{\text{Si}}$	185	1.69	184	1.67	183	1.73
1- $V_{\text{Si}}V_{\text{C}}$	216	2.39	216	2.40	214	2.44
2- $V_{\text{Si}}V_{\text{C}}$	254	3.48	-	-	-	-
3- $V_{\text{Si}}V_{\text{C}}$	286	4.27	-	-	-	-
4- $V_{\text{Si}}V_{\text{C}}$	321	4.94	-	-	-	-

In order to compare the results obtained here by the semiconductor model, in which the lack of complete positron screening is taken into account by means of the high-frequency dielectric constant [see Eq. (4)], with the insulator model,<sup>32</sup> it is assumed, to a first approximation, that the enhancement of the electron density at the positron is proportional to the atomic polarizability  $\alpha_{\text{at}}$ , which has been estimated by the Clausius-Mossotti relation. The corresponding positron annihilation rate  $\lambda^{\text{IN}}$  is thereby written as

$$\lambda^{\text{IN}} = 1/\tau^{\text{IN}} = \lambda^{\text{IPM}} [1 + A + B\Omega(\epsilon_{\infty} - 1)/(\epsilon_{\infty} + 2)], \quad (5)$$

where  $\lambda^{\text{IPM}}$  is the positron annihilation rate calculated within the independent particle model and  $\Omega$  represents the unit-cell volume. The constants  $A (=0.648)$  and  $B (=0.024)$  are parameters obtained by fitting the calculated positron lifetimes<sup>32</sup> to experimental lifetimes which are known for different insulators. Following this model the bulk lifetime obtained for 3C-SiC amounts to 166 ps, and the lifetimes corresponding to 2H- and 6H-SiC are 168 and 165 ps, respectively. These calculated lifetime values for different polytypes of SiC and those from Ref. 32 are more than 20 ps longer than the experimental bulk lifetime for 6H-SiC. Therefore, we cannot rely on the insulator model to describe SiC and shall use the results obtained by using the semiconductor model, as described above.

The binding energies for positrons trapped by a vacancy-type defect are collected in Table II. The lifetimes calculated in the neutral, unrelaxed mono- and divacancies are also quite similar in the three polytypes. Therefore, the zinc-blende structure has also been used to perform the calculations in larger vacancy agglomerates.

The vacancy agglomerates were formed by taking away from the simulated zinc-blende structure the closest Si-C pairs of atoms. The increase of the positron lifetime from the bulk state to the vacancy state is quite small for C monovacancies, but larger for Si monovacancies; the ratio of lifetimes for positrons in monovacancies and in bulk SiC is 1.07 for C and 1.31 for Si. Even though these ratios are smaller than those for metals (1.5 – 1.6), the ratio corresponding to Si in SiC is larger than those for elemental (Ge, Si) and compound (II-VI, III-V) semiconductors. Therefore, the localization of the positron in the silicon vacancy  $V_{\text{Si}}$  in SiC should be greater than in the other semiconductors, but less than in metal monovacancies. However, in SiC divacancies the localization is similar to that in metal monovacancies.

The binding energy  $E_b$  of the positron to defects (see Table II) is fairly small for  $V_{\text{C}}$  but relatively large for  $V_{\text{Si}}$ . However, one has to bear in mind that, unlike the positron lifetimes, the positron binding energy to a defect is quite sensitive to the self-consistency of the electronic structure. Moreover, if the effects due to the localized positron were included self-consistently, the positron binding energy would increase due to the increase of the average electron density<sup>24</sup> and the lattice relaxation at the defect.<sup>33</sup>

### B. Variable-energy positron measurements: Doppler broadening spectroscopy

$S(E)$  results for all specimens are presented in Fig. 1. The data suggest that the samples belong to one of three groups.

Group 1: (EU0) represents the virgin specimen, which is characterized by a bulk parameter value  $S_b = 0.470 \pm 0.001$  and an effective positron diffusion length  $L_+ = (36.5 \pm 1.8)$  nm. This value of  $L_+$  is considerably shorter than that quoted for perfect Si;<sup>34</sup> the reason for this is currently unclear, but may perhaps be associated with shallow trapping at C sites, or be the results of a near-surface electric field. The presence of the latter could be checked in the future by performing high-temperature measurements (the facility for which was not available during the present experiment).

Group 2: (EU1, 2, 3, 4, and 5) contains specimens whose crystalline structure has not been lost as a result of damage caused by ion implantation. The  $S$ - $E$  relations show that positrons are sensitive to the damage caused by different flu-

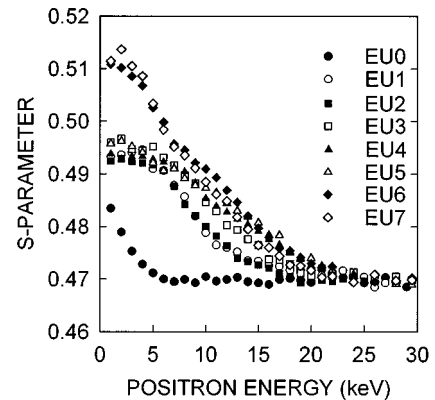


FIG. 1. Mean Doppler broadening parameter  $S$  as a function of incident positron energy  $E$  for specimens EU0–EU7.

TABLE III. Thickness  $d$  (measured from the surface) of damaged (DL) and amorphous (AL) layers in 6H-SiC specimens implanted with 200-keV Ge<sup>+</sup> ions for different fluences  $\Phi$ . The diffusion length used throughout was 36.5 nm, as found for specimen EU0.

Specimen	$\Phi$ (m <sup>-2</sup> )	No. layers	$d_{AL}$ (nm)	$d_{DL}$ (nm)
EU0	-	1	-	-
EU1	$1 \times 10^{16}$	2	-	339 (5)
EU2	$3 \times 10^{16}$	2	-	344 (5)
EU3	$1 \times 10^{17}$	2	-	428 (5)
EU4	$3 \times 10^{17}$	2	-	566 (6)
EU4	$3 \times 10^{17}$	3	11 (10)	560 fixed
EU5	$1 \times 10^{18}$	2	-	596 (6)
EU5	$1 \times 10^{18}$	3	57(10)	560 fixed
EU6	$3 \times 10^{18}$	3	124(4)	619 (6)
EU7	$1 \times 10^{19}$	3	133(3)	552 (6)

ences of implanted ions; it should be possible to characterize such damage even at fluences much lower than  $10^{16}$  ions m<sup>-2</sup>. For comparison, in the case of Si implanted with 540-keV Si ions the slow positron technique has been found to be sensitive to levels of damage of the form of open-volume defects approximately 2 orders of magnitude below the minimum detectable by ion channeling.<sup>35</sup> (The latter technique is more sensitive to interstitial defects and as such is complementary to positron annihilation.)

Group 3: (EU 6 and 7) contains those specimens whose crystalline structure has been partly lost as a result of ion implantation, and in which TEM work has demonstrated the existence of an amorphous layer at the surface.<sup>18</sup> This is reflected in the much higher  $S$  values observed in the energy range 0.1–7 keV for this group, compared with those in group 2.

The thicknesses of the damaged layers then have been evaluated using the program VEPFIT 5 (Ref. 21) with two or three layers (for group 2 and group 3 specimens, respectively). The values  $S_b$  and  $L_+$  deduced for specimen EU0 were used in the analysis of data for all the other specimens; electric fields were assumed to be zero. VEPFIT assumes that layers have sharp boundaries and are homogeneous. The results are summarized in Table III. An increase of the damaged crystalline layer thickness with increasing fluence up to  $\Phi = 3 \times 10^{17}$  m<sup>-2</sup> is found. In addition, for the two highest fluences the thickness of the amorphous surface layer was found to be about 130 nm; this thickness corresponds well to the value of 160 nm measured for specimen EU7 by TEM.<sup>18</sup> Positron diffusion lengths in the defected and amorphous layers were found by VEPFIT to be 13 and 0.5 nm, respectively, pointing to much increased positron trapping probabilities in these layers.

Three-layer fits to the EU4 and EU5 data, with the thickness of the damaged crystalline layer fixed at 560 nm, suggest the possible presence of thin surface amorphous layers of approximate thicknesses 20 and 60 nm, respectively. More precise determination of these thicknesses would require finer energy steps in the low- $E$  data; remeasurement was not possible because immediately after the measurements all specimens were cut and studied further in other laboratories in the European Network.

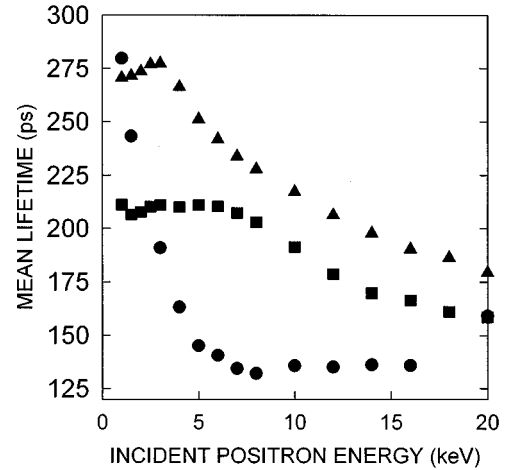


FIG. 2. Mean positron lifetime  $\tau$  as a function of incident positron energy  $E$  for a virgin 6H-SiC sample (●) and specimens EU3 (■) and EU7 (▲).

### C. Variable-energy positron measurements: Lifetime spectroscopy

To gain more insight into the nature of the vacancy-type defects produced by ion-implantation timed positron beam measurements in the energy range 1–20 keV have been performed for specimens EU3 and EU7. As the virgin specimen EU0 was no longer available another virgin 6H-SiC specimen was measured for comparison. The lifetime spectra contained about  $10^6$  events and were analyzed using a modified version of the program package POSITRONFIT (Ref. 36) using a stable, measured resolution function of 250-ps FWHM. The mean lifetime results  $\tau(E)$  are shown in Fig. 2, and show trends similar to those seen in  $S(E)$  in Fig. 1, as expected. By comparison of the data for the virgin reference specimens in Figs. 1 and 2 one sees that  $S(E)$  and  $\tau(E)$  have a similar energy dependence; thus the diffusion length deduced from  $\tau(E)$  is in agreement with that from  $S(E)$  quoted above.

In virgin 6H-SiC no straightforward one-component fit is possible. This is due to a side peak close to the main lifetime spectrum for low incident energies. This feature, due to re-emitted slow positrons returned to and annihilated at the sample<sup>37</sup> necessitates a three-component fit (with the third artificial long lifetime component in the ns range). However, by using data in the energy range 5–20 keV, eliminating the long component, and averaging the mean lifetimes obtained by the multicomponent fits, an estimate of the bulk lifetime value  $\tau_b = (140 \pm 5)$  ps is obtained, in rather good agreement with the theoretical calculation (see Table I). No measurable slow-positron reemission was seen from the defected samples EU3 and EU7, and the resultant absence of the side peak in the lifetime spectra meant that analysis could easily be carried out over the whole range of incident positron energies for these samples.

In the case of specimen EU3 an unconstrained two-component fit yielded a longer lifetime component  $\tau_2$  which is plotted, along with its intensity  $I_2$ , as a function of  $E$  in Fig. 3. We regard the mean lifetime ( $235 \pm 3$ ) ps obtained from data between 1.5 and 14 keV to be representative of divacancies created by ion implantation in crystalline SiC

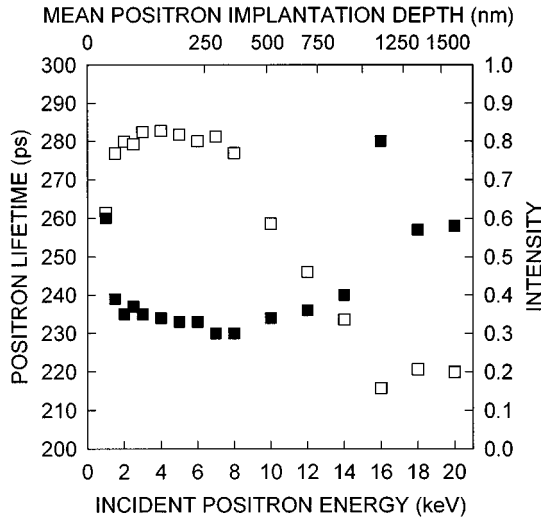


FIG. 3. Second positron lifetime  $\tau_2$  (■, left y axis) and intensity  $I_2$  (□, right y axis) as a function of incident positron energy  $E$  for specimen EU3.

(see Table II). The small discrepancy between measured and calculated  $\tau_2$  values may arise from atomic relaxation around the defect; the calculated positron lifetimes in this study correspond to neutral, unrelaxed defects, whereas vacancies in semiconductors might be in different charge states, which affect the positron lifetime through atomic relaxation.<sup>33,38,39</sup> The existence of such states could be verified by performing low-temperature measurements; facilities for such measurements were not, however, available in the present experiment. Moreover, the relaxation around the defect is expected to increase with the number of vacancies in the agglomerate.

The results of an unconstrained two-component fit to the lifetime data for specimen EU7 are shown in Fig. 4. The fit gives a longer lifetime component  $\tau_2 = (305 \pm 6)$  ps, with intensities up to about 80%, in the energy range 1–5 keV. Calculations suggest that this lifetime should result from annihilations in vacancy clusters consisting of at least four but

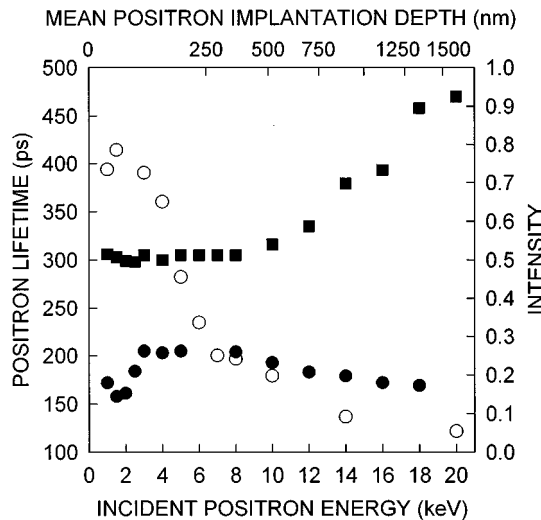


FIG. 4. Positron lifetimes  $\tau_1$  and  $\tau_2$  (● and ■, respectively, left y axis) and intensity  $I_2$  (○, right y axis) as a function of incident positron energy  $E$  for specimen EU7.

more probably six vacancies. Such clusters, not expected in amorphous layers produced by other methods such as rapid quenching, sublimation, etc., clearly arise in this case as a result of the high-fluence ion bombardment. The rise in  $\tau_2$  at higher energies should not be considered significant as  $I_2$  decreases to a few percent and fitting uncertainties are high. The shorter lifetime component decreases from about 220 to 163 ps as the incident positron energy increases from 5 to 20 keV; this may reflect an averaging of annihilations in the bulk and a defect having a lifetime of the order (200–250) ps, i.e., the divacancy. However, a consistent spectrum analysis with three lifetimes (representing a trapping-reduced bulk annihilation component and two defect components) was impossible, even with constraints on one lifetime. This effect, arising from the relatively broad resolution function, of 250-ps FWHM, is well known in conventional lifetime measurements and leads to the two-defect trapping model.<sup>40</sup> In order to clarify the picture the analysis of the EU7 data has been repeated using this model with a fixed  $\tau_2 = 305$  ps, and the results of this constrained fitting procedure are discussed in the following section.

#### D. Estimation of defect concentrations from $\tau(E)$

For sample EU3 unconstrained two-component fits (yielding lifetimes  $\tau_1$  and  $\tau_2$  with intensities  $I_1$  and  $I_2$ ) could not yield a value for the bulk lifetime  $\tau_b$  close to the expected value of 141 ps (Table I) by using the one-defect trapping model<sup>41</sup> according to

$$\tau_b = (I_1/\tau_1 + I_2/\tau_2)^{-1}. \quad (6)$$

This suggests that positrons sample a second type of defect in the implanted material, and that in order to obtain trapping rates and hence estimate defect concentrations one has to apply the two-defect trapping model to the lifetime data for both specimens EU3 and EU7.

When a specimen contains two types of defects and the lifetime spectrum has been decomposed into two lifetimes only, the positron trapping rates into the defects can be calculated<sup>40</sup> from the equations

$$k_v = [\tau_1(\lambda_f - I_2\lambda_{cl}) - I_1]/(\tau_v - \tau_1), \quad (7)$$

and

$$k_{cl} = (I_2/I_1)(\lambda_f - \lambda_{cl} + k_v). \quad (8)$$

Here  $k_{cl}$  denotes the trapping rate into the vacancy clusters and decaying with lifetime  $\tau_{cl} = I/\lambda_{cl}$ ;  $k_v$  is the trapping rate into the other defect.

The two-defect trapping model has been applied to the results of the two-component fits to the  $\tau(E)$  data for specimen EU3, with (a)  $\tau_{cl}$  fixed at 235 ps and (b) the second defect assumed to be the Si vacancy  $V_{Si}$  ( $\tau_v = 183$  ps, see Table II). With a bulk lifetime  $\tau_b = 141$  ps (Table I) the trapping rates into mono- and divacancies,  $k_v$  and  $k_{2v}$ , respectively, have been evaluated at every incident positron energy  $E$ . The results are presented in Fig. 5.

A similar treatment has been applied to the EU7 data, with  $\tau_{cl}$  fixed at 305 ps,  $\tau_b = 141$  ps and assuming the second defect to be the divacancy  $V_{Si}V_C$  ( $\tau_{2v}$  measured to be 235 ps, see Sec. III C). Thus the trapping rates into divacancies and

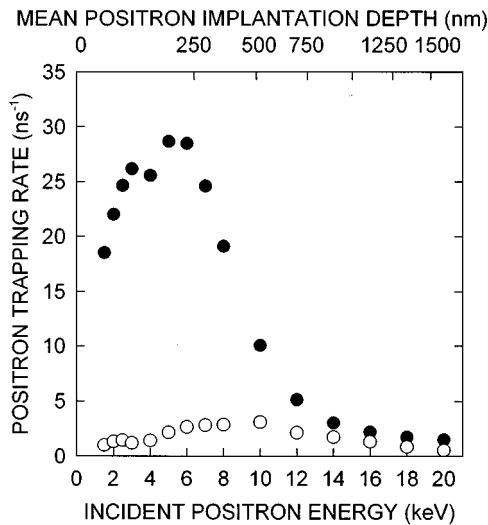


FIG. 5. Trapping rates into mono- and divacancies,  $k_v$  (○) and  $k_{2v}$  (●), respectively, as a function of incident positron energy  $E$  for specimen EU3. Note that these results are based on experimental data and do not represent a fit.

vacancy clusters,  $k_{2v}$  and  $k_{cl}$ , respectively, have been evaluated. The results are presented in Fig. 6.

In order to extract average defect concentrations for the damaged layers one should first consider the positron implantation profiles  $P(E, z)$ . The mean implantation depth  $\langle z \rangle$  (in nm) is approximated by<sup>21</sup>

$$\langle z \rangle = (40/\rho)E^{1.62}, \quad (9)$$

where  $E$  is in keV and  $\rho$  is the mass density ( $3.217 \text{ g cm}^{-3}$  for SiC). It can be deduced by reference to Table III that for values of  $E$  below about 6 keV essentially all of the implanted positrons stop in the damaged crystalline layer in specimen EU3; the equivalent energies for specimen EU7 are 3 keV for the amorphous layer and 7 keV for the damaged crystalline layer. If we assume that the defects are uni-

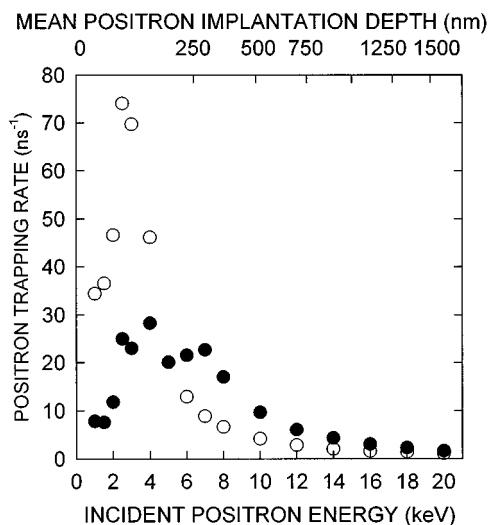


FIG. 6. Trapping rates into divacancies and vacancy clusters,  $k_{2v}$  (●) and  $k_{cl}$  (○), respectively, as a function of incident positron energy  $E$  for specimen EU7.

formly distributed in these layers, their concentrations  $c$  may be estimated. By reference to Figs. 5 and 6 one obtains the value of  $k_{2v}$  characteristic of the damaged crystalline layer in EU3 is  $2.8 \times 10^{10} \text{ s}^{-1}$ , and for EU7 the trapping rates are  $7.5 \times 10^{10} \text{ s}^{-1}$  for clusters and  $3 \times 10^{10} \text{ s}^{-1}$  for divacancies. Such high calculated trapping rates are evidence for near-saturation trapping of positrons in both defective layers if one considers a trapping rate of the order of  $10^{11} \text{ s}^{-1}$  to be the sensitivity limit of PAS.

To deduce  $c$  one must first know the value for the specific trapping rate  $\mu$  for each type of defect; then  $c = k/\mu$ . Such data do not exist for 6H-SiC and so, as a first approximation, the known value for monovacancies in Si  $\mu_v = 3 \times 10^{14} \text{ s}^{-1}$  (Ref. 42) is used. Furthermore, it is assumed that  $\mu_{nv} = n\mu_v$  for a cluster of  $n$  vacancies ( $n < 8$ ); hence we shall use  $\mu_{2v} = 6 \times 10^{14} \text{ s}^{-1}$  and  $\mu_{cl} = 1.8 \times 10^{15} \text{ s}^{-1}$ . For metal vacancy clusters in iron<sup>43</sup> experimental evidence suggests that such an assumption underestimates the positron trapping at the vacancy clusters; this might also be true for 6H-SiC, and so the defect concentrations deduced here should be considered to be only a first approximation. They are 47 ppm divacancies in the damaged layer in specimen EU3 and 42 ppm clusters and 50 ppm divacancies in the damaged regions in specimen EU7.

The knowledge of the true defect profile  $D(z)$  is important in semiconductor technology for devices design. However, one should recognize that the distributions  $k(z)$  presented in Figs. 5 and 6 represent at each energy  $E$  a convolution of the true defect profile  $D(z)$  with the positron implantation profile  $P(E, z)$  corresponding to the  $E$  value, and then only if (i) any positron diffusion from low-defective to high-defective regions is neglected, and (ii) no internal electric fields affect the measured defect intensities. In general, the extraction of the true (defect) profile in any positron beam study represents an inversion problem of the form

$$k(E) = \mu \int_0^\infty P(E, z) D(z) dz. \quad (10)$$

The solution of such a problem is not straightforward and requires the application of properly formulated boundary conditions. The model-free deconvolution of depth profiles obtained by positron beams of variable energy has been recently discussed and summarized.<sup>44</sup> It is planned to develop the application of such a procedure to our data in the future.

From the comparison of our  $S(E)$  data with the results of TRIM90 code calculations it is clear that even if the deconvolution problem is neglected the measured defect profiles  $D(z)$  extend beyond those indicated by the Monte Carlo simulations, which predict vacancy formation up to a depth of 150–200 nm. This may be due to defects forming in front of the implanted ions, and/or the effects of channeling;<sup>45</sup> further experimental and theoretical work is warranted.

### E. Comparisons with other work

Mokrushin *et al.*<sup>46</sup> studied defects in  $n$ -irradiated 6H-SiC, with homogeneously distributed radiation damage, by conventional lifetime spectroscopy. These authors attributed a lifetime of  $(225 \pm 3) \text{ ps}$  to positrons annihilated in divacancies, whereas the values  $(360 \pm 15) \text{ ps}$  and  $(463 \pm 18) \text{ ps}$

should correspond to positrons in clusters of 5–8 and >20 vacancies, respectively. We regard the divacancy value to be in very good agreement with our experimental result. According to Table II we would ascribe the lifetime  $\tau_{cl}=360$  ps to a cluster of 8 vacancies, also in agreement with the result of Ref. 25. Mokrushin *et al.* suggest that vacancy clustering due to postirradiation thermal annealing is linked with the  $N^+$  dopant concentration.

Dannefaer *et al.*<sup>11,16</sup> attributed their measured lifetimes of 160 and 260–270 ps to annihilation in irradiation-induced monovacancies (i.e.,  $V_C$  and  $V_{Si}$ , respectively). The differences between their interpretation and that of the present work may lie in their use of the insulator model (see Sec. III A). The theoretical results of Table II suggest that their experimental lifetime value of 260–270 ps does not correspond to Si monovacancies but could most probably be due to quadrivacancies of the type-2  $V_{Si}V_C$ .

It is not surprising but interesting to note that the temperature during electron irradiation seems to play an important role in the formation of vacancy agglomerates, presumably due to the temperature dependence of defect mobility. Whereas at 80 K the main result seems to be the divacancy,<sup>14,15</sup> irradiation at energies above 2.2 MeV at room temperature results in larger aggregates.<sup>11,16</sup> On the other hand, 80-K irradiation by 0.47-MeV electrons, whose energy is just above the displacement threshold,<sup>14</sup> results in the production of monovacancies.

#### IV. CONCLUSIONS

The theoretical and experimental studies presented herein have demonstrated that the vacancy-type damage caused by ion implantation in 6H-SiC can be monitored and well characterized by positron annihilation. In particular it appears that the predominant defect is the divacancy, whose formation by irradiation has been assumed for a number of years following optical investigations;<sup>47</sup> the present positron measurements, however, are the first direct proof of its existence.

In the fluence range  $10^{16}$ – $10^{18}$  ions  $m^{-2}$  it has been

found that in addition to divacancies a certain concentration of Si monovacancies should exist. Defect profiles have been presented and these have been converted into concentration profiles based on plausible assumptions.

In the fluence range  $3 \times 10^{18}$ – $10^{19}$  ions  $m^{-2}$  the existence of an amorphous surface layer is deduced from the nondestructive positron measurements. Its thickness has been evaluated and compared to the results of destructive test methods. There is generally good agreement between the results. Furthermore, the positron results indicate the existence of larger vacancy clusters in the amorphous surface layer. These clusters consist of at least four but more probably six vacancies and are very attractive to positrons. Depth profiles of these large clusters have also been presented.

The investigations have indicated that PAS should be able to monitor and characterize the radiation damage caused by ion implantation into 6H-SiC even at fluences below  $10^{16}$  ions  $m^{-2}$ . For comparison, in Si it has been found that the slow positron technique is sensitive to levels of damage approximately 2 orders of magnitude below the minimum detectable by ion channeling.

The combination of different slow positron beam techniques coupled with updated theoretical evaluations presents a rather clear picture of the vacancy-type defects created by ion implantation and allows one to suggest ways to explain contradictions in the interpretation of earlier results.

The problem of deriving the true defect profile  $D(z)$  from the experimental profiles referred to above has been discussed but this needs further extensive work, which is currently in progress. However, it seems that even without further analysis one can state that these profiles are more extended into the material than indicated by TRIM code calculations.

#### ACKNOWLEDGMENT

This work was partly supported by EMRS-Network 3:IBOS (Contract No. ERBCHRX-CT93-0125).

<sup>1</sup>G. Pensl and R. Helbig, in *Festkörperprobleme*, Advances in Solid State Physics Vol. 30, edited by U. Rössler (Vieweg, Braunschweig, 1990), pp. 133–156.

<sup>2</sup>G. Pensl and W. Choyke, *Physica B* **185**, 264 (1993).

<sup>3</sup>L. Patrick, *Phys. Rev. B* **5**, 2198 (1972).

<sup>4</sup>*Positrons in Solids*, edited by P. Hautojärvi, Topics in Current Physics Vol. 12 (Springer, Berlin, 1979).

<sup>5</sup>*Positron Solid State Physics*, Proceedings of the International School of Physics “Enrico Fermi,” Course LXXXIII, Varenna, 1981, edited by W. Brandt and A. Dupasquier (North-Holland, Amsterdam, 1983).

<sup>6</sup>P. J. Schultz and K. G. Lynn, *Rev. Mod. Phys.* **60**, 701 (1988).

<sup>7</sup>*Positrons at Metallic Surfaces*, edited by A. Ishii (Trans. Tech. Publications, Aedermannsdorf, 1992).

<sup>8</sup>P. Hautojärvi, *Mater. Sci. Forum* **175-178**, 47 (1995).

<sup>9</sup>M. Forster, W. Claudy, H. Hermes, M. Koch, K. Maier, J. Major, H. Stoll, and H.-E. Schaefer, *Mater. Sci. Forum* **105-110**, 1005 (1992).

<sup>10</sup>W. Puff, M. Boumerzoug, J. Brown, P. Mascher, D. Macdonald, P. J. Simpson, A. G. Balogh, H. Hahn, W. Chang, and M. Rose, *Appl. Phys. A* **61**, 55 (1995).

<sup>11</sup>S. Dannefaer, *Appl. Phys. A* **61**, 59 (1995).

<sup>12</sup>H. Itoh, M. Yoshikawa, I. Nashiyama, L. Wei, S. Tanigawa, S. Misawa, H. Okumura, and S. Yoshida, *Hyperfine Interact.* **79**, 725 (1993).

<sup>13</sup>A. I. Girka, A. D. Mokrushin, E. N. Mokhov, S. V. Svirida, and A. V. Shishkin, in *Amorphous and Crystalline Silicon Carbide III*, edited by G. L. Harris, M. G. Spencer, and C. Y. Yang, Springer Proceedings in Physics Vol. 56 (Springer, Berlin, 1992), pp. 207–211.

<sup>14</sup>A. A. Rempel, H.-E. Schaefer, M. Forster, and A. I. Girka, in *Covalent Ceramics II: Non-Oxides*, edited by A. R. Barron, G. S. Fishman, M. A. Fury, and A. F. Hepp, MRS Symposia Proceedings No. 327 (Materials Research Society, Pittsburgh, 1994), pp. 299–304.

<sup>15</sup>A. A. Rempel and H.-E. Schaefer, *Appl. Phys. A* **61**, 51 (1995).

- <sup>16</sup>S. Dannefaer, D. Craigen, and D. Kerr, *Phys. Rev. B* **51**, 1928 (1995).
- <sup>17</sup>C. J. McHargue and J. M. Williams, *Nucl. Instrum. Methods B* **80/81**, 889 (1993).
- <sup>18</sup>V. Heera, J. Stoemenos, R. Kögler, and W. Skorupa, *J. Appl. Phys.* **77**, 2999 (1995).
- <sup>19</sup>Cree Research Inc., Durham, NC.
- <sup>20</sup>N. B. Chilton and P. G. Coleman, *Meas. Sci. Technol.* **6**, 53 (1995).
- <sup>21</sup>A. van Veen, H. Schut, J. de Vries, R. A. Hakvoort, and M. R. Ijpma, in *Positron Beams for Solids and Surfaces*, edited by P. J. Schultz, G. R. Massoumi, and P. J. Simpson, AIP Conf. Proc. No. 218 (AIP, New York, 1990), p. 171.
- <sup>22</sup>P. Willutzki, J. Störmer, G. Kögel, P. Sperr, D. T. Britton, R. Steindl, and W. Triftshäuser, *Meas. Sci. Technol.* **5**, 548 (1994).
- <sup>23</sup>M. J. Puska and R. M. Nieminen, *J. Phys. F* **13**, 333 (1983).
- <sup>24</sup>E. Boronski and R. M. Nieminen, *Phys. Rev. B* **34**, 3820 (1986).
- <sup>25</sup>J. Arponen and E. Pajanne, *J. Phys. F* **9**, 2359 (1979).
- <sup>26</sup>D. M. Ceperley and B. J. Alder, *Phys. Rev. Lett.* **45**, 566 (1980).
- <sup>27</sup>J. Perdew and A. Zunger, *Phys. Rev. B* **23**, 5048 (1981).
- <sup>28</sup>R. W. G. Wyckoff, *Crystal Structures* (Wiley, New York, 1963), Vol. 1, pp. 111 and 113.
- <sup>29</sup>G. E. Kimball and G. H. Shortley, *Phys. Rev.* **45**, 815 (1934).
- <sup>30</sup>M. J. Puska, *J. Phys.: Condens. Matter* **3**, 3455 (1991).
- <sup>31</sup>L. Patrick and W. J. Choyke, *Phys. Rev. B* **2**, 2255 (1970).
- <sup>32</sup>M. J. Puska, S. Mäkinen, M. Manninen, and R. M. Nieminen, *Phys. Rev. B* **39**, 7666 (1989).
- <sup>33</sup>K. Laasonen, M. Alatalo, M. J. Puska, and R. M. Nieminen, *J. Phys.: Condens. Matter* **3**, 7217 (1991).
- <sup>34</sup>P. Asoka-Kumar, K. G. Lynn, and D. O. Welsh, *J. Appl. Phys.* **76**, 4935 (1994).
- <sup>35</sup>I. V. Mitchell, P. J. Simpson, P. J. Schultz, M. Vos, U. Akano, and C. Wu, in *Positron Beams for Solids and Surfaces* (Ref. 21), p. 121.
- <sup>36</sup>P. Kirkegaard and M. Eldrup, *Comput. Phys. Commun.* **7**, 401 (1974).
- <sup>37</sup>J. Störmer, A. Goodyear, W. Anwand, G. Brauer, P. G. Coleman, and W. Triftshäuser, *J. Phys.: Condens. Matter* **8**, L89 (1996).
- <sup>38</sup>M. J. Puska, O. Jepsen, O. Gunnarson, and R. M. Nieminen, *Phys. Rev. B* **34**, 2695 (1986).
- <sup>39</sup>S. Mäkinen and M. J. Puska, *Phys. Rev. B* **40**, 12 523 (1989).
- <sup>40</sup>A. Vehanen, P. Hautojärvi, J. Johansson, J. Yli-Kauppila, and P. Moser, *Phys. Rev. B* **25**, 752 (1982).
- <sup>41</sup>W. Brandt, *Appl. Phys.* **5**, 1 (1974).
- <sup>42</sup>S. Dannefaer, *Phys. Status Solidi A* **102**, 481 (1987).
- <sup>43</sup>P. Hautojärvi, L. Pöllänen, A. Vehanen, and J. Yli-Kauppila, *J. Nucl. Mater.* **114**, 250 (1983).
- <sup>44</sup>G. Kögel, *Mater. Sci. Forum* **175-178**, 185 (1995).
- <sup>45</sup>S. Ahmed, C. J. Barbero, T. W. Sigmon, and J. W. Erickson, *J. Appl. Phys.* **77**, 6194 (1995).
- <sup>46</sup>A. D. Mokrushin, A. I. Girka, and A. V. Shishkin, *Phys. Status Solidi A* **128**, 31 (1991).
- <sup>47</sup>W. J. Choyke, *The Physics and Chemistry of Carbides, Nitrides and Borides*, Vol. 185 of NATO Advanced Study Institute (Kluwer, Dordrecht, 1990), p. 563.